Diagn Interv Radiol 2010; 16:134–144

ABDOMINAL IMAGING

REVIEW

Multidetector CT technique and imaging findings of urinary stone disease: an expanded review

Barış Türkbey, Erhan Akpınar, Çiğdem Özer, Evrim Bengi Türkbey, Volkan Eken, Muşturay Karçaaltıncaba, Okan Akhan

ABSTRACT

Unenhanced computed tomography (CT) is currently being widely used for the evaluation of patients presenting with acute flank pain. A variety of primary and secondary findings detected on unenhanced CT contribute not only to the diagnosis but also to the treatment plan. This review includes primary and secondary multidetector CT imaging findings of urinary stone disease, potential pitfalls with exquisite images of sample cases, and a brief review of radiation dose reduction and contrast administration strategies.

Key words: • *urinary tract stones* • *computed tomography* • *flank pain*

From the Department of Radiology (B.T. ✉ *bturkbey@yahoo.com*), Hacettepe University School of Medicine, Ankara, Turkey.

Received 22 December 2008; revision requested 29 December 2008; revision received 30 December 2008; accepted 31 December 2008.

Published online 9 October 2009
DOI 10.4261/1305-3825.DIR.2187-08.3

Acute flank pain is a common clinical entity that can be secondary to urinary and extraurinary causes; urinary stone disease appears to be the most common cause and affects 3–5% of population in the Western world (1). An ideal imaging modality should provide information about not only the presence or absence of urinary tract stones but also about its size, site, composition, and related complications such as obstruction. Optimum radiological evaluation has a central role in the management of patients with acute flank pain (2–4).

Urinary stone disease affects males twice as females and peaks around the age of 30 years in males and between 35 and 55 years among females. Several conditions were identified as predisposing risk factors such as positive family history, geography, diet, obesity, recurrent urinary tract infection, insulin resistance, prolonged immobilization; moreover, specific entities such as idiopathic hypercalciuria, secondary hypercalciuria, hyperuricosuria, and type 1 renal tubular acidosis were also defined (5). Urinary tract stones vary according to their chemical composition: 34% of them consist of calcium oxalate and phosphate, 33% consist of pure calcium, 6% of pure calcium phosphate, 15% mixed struvite and apatite, 8% uric acid, and 1% cystine (6).

The common symptoms of urinary stone disease are colicky pain and hematuria. Pain generally starts suddenly in the flank region and increases rapidly often requiring analgesics for relief; as time passes pain may radiate to lower abdomen, into scrotum or labia as stone moves distally within the urinary tract (2, 7). Other symptoms may include nausea, vomiting, and dysuria (7).

Unenhanced multidetector computed tomography (MDCT) in the diagnosis of urinary stone disease

Imaging indications for urinary stone disease are: i) to establish the diagnosis; ii) to assess the stone burden within the urinary system; iii) to determine the pelvicalyceal anatomy; iv) to plan the treatment; v) to evaluate the outcome of treatment; vi) to assess the complications (8).

Basic principles and technique

In 1995 Smith et al. introduced unenhanced helical computed tomography (CT) as an initial imaging modality for patients with acute flank pain referred for urinary stone disease management (9). Since then, unenhanced helical CT has been widely accepted as a rapid and accurate diagnostic imaging modality replacing other techniques (10). Unenhanced CT is not a standard abdomen CT imaging procedure, and it avoids the use of intravenous contrast material and its potential hazards (11–13).

Unenhanced MDCT parameters dedicated for imaging evaluation of urinary stone disease in our institution are: detector collimation, 2 x 2.5 mm, 4 x 2.5 mm, 16 x 1.5 mm, 64 x 0.7 mm; slice thickness, 3 mm;

Figure 1. Abdominal topogram shows the scanned range in an unenhanced CT examination dedicated for the detection of urinary tract stones.

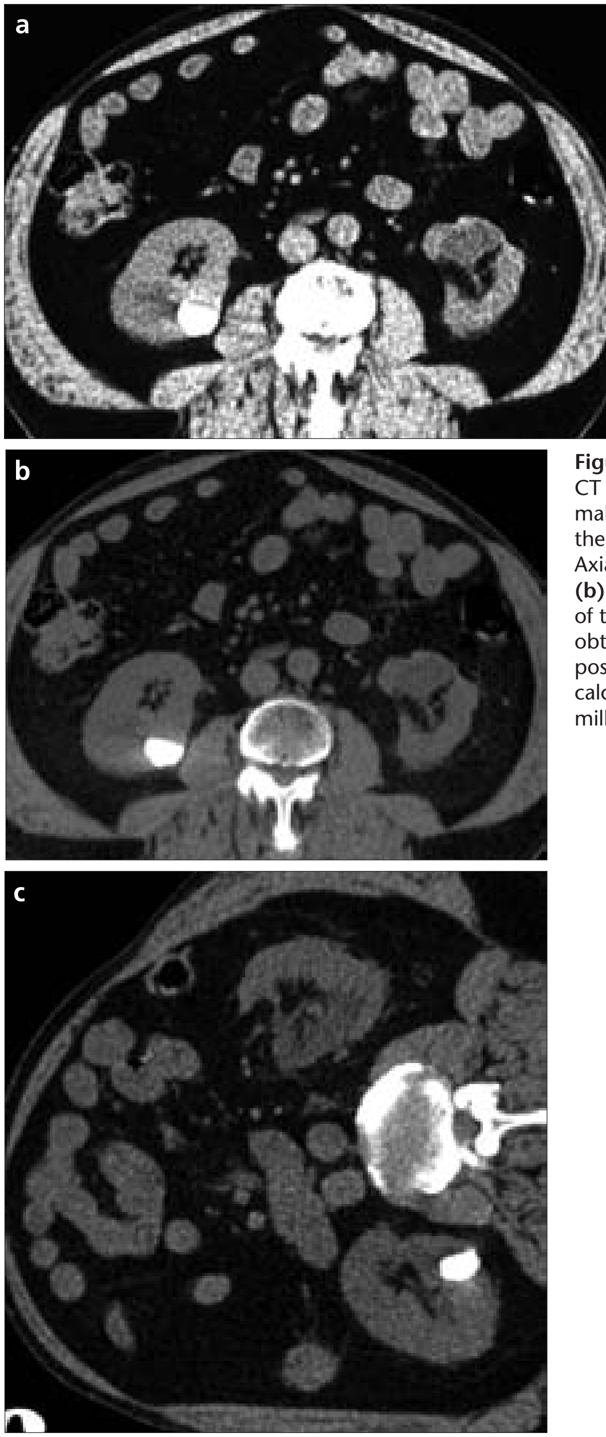

Figure 2. a–c. Axial unenhanced CT image **(a)** of a 34-year-old male shows milk of calcium within the right kidney collecting system. Axial CT image at bone window **(b)** shows dense calcified nature of the lesion. Axial CT image obtained at the right decubitus position **(c)** shows leveling of the calcified material, consistent with milk of calcium.

pitch, 1.5; mAs, 80; kVp, 130. Scanning is almost always performed in supine position and images are obtained from the top of the kidneys through the base of the urinary bladder in a single breath hold (Fig. 1). Images at prone or left/right decubitus positions can be obtained if needed (Fig. 2). In cases where a stone is identified in the ureterovesical junction prone imaging can be added to the protocol, this technique lets the stone to float freely within the bladder if it is not located at the ureterovesical junction (Fig. 3); additionally, differentiation of a urinary bladder mass from a clot can be made via this approach.

In addition to axial images obtained by unenhanced MDCT, it is possible to obtain more detailed coronal, sagittal multiplanar reconstructions (MPR), and 3D reconstruction images (Fig. 4). In this manner, obtaining additional scans and radiation exposure are avoided. Moreover, by intravenous contrast material administration, intravenous pyelogram (IVP) like images can be reconstructed (8).

Radiation dose optimization and dose reduction: ALARA (as low as reasonably achievable)

Radiation dose optimization is a growing concern among radiologists, particularly in children and young adults. Patients with urinary stone disease may experience repeated stone formations and therefore they may undergo multiple CT examinations during their life span. The radiation dose of CT has to be optimized in order to prevent undesired effects of radiation in this group of patients.

Ways of reducing radiation exposure can be grouped under three main topics, namely re-adjustment of CT scanning parameters, modulation of CT scanning parameters, and technologic advances for radiation dose reduction.

Firstly, readjustment of CT scanning parameters such as current and voltage, table speed, pitch and shielding should be discussed. The reduction in tube current is the most practical means of reducing the radiation dose. In previous studies, authors suggested that it is possible to reduce tube current without markedly affecting image quality

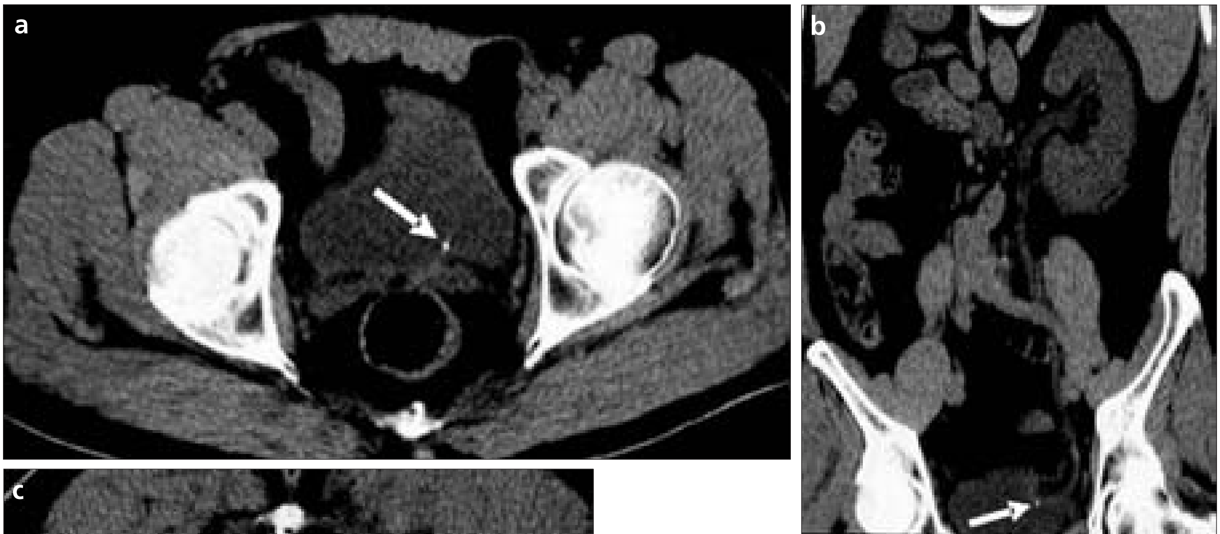

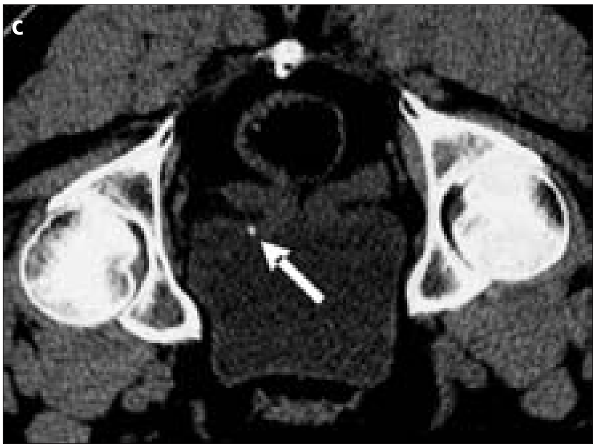

Figure 3. a–c. Axial **(a)** and coronal reconstructed **(b)** CT images of a 40-year-old female show a left ureterovesical junction stone *(arrow)*. The stone located at the left ureterovesical junction does not change its location on image obtained in prone position (*arrow,* **c**).

(14–18). A study has shown that in patients with suspected renal colic who weighed less than 90 kg unenhanced helical CT performed at a reduced tube current demonstrated a higher accuracy when compared with that of the standard technique (19). As for pitch, an increase in pitch decreases duration of examination and also decreases radiation exposure to the body. Although increase of pitch causes helical artifacts and decreased spatial resolution, some investigators have reported using a pitch of 2 or above with satisfactory results in cases of suspected renal colic (20, 21).

Secondly, as a modulation of scanning parameters, tube current modulation according to patient weight and cross-sectional abdominal dimensions is a common way of reducing radiation exposure. Recent studies have revealed that in children and adults tube current can be reduced on the basis of patient weight with acceptable image quality (22, 23).

Lastly, technologic advances for radiation reduction which include X-ray filtration and automatic modulation

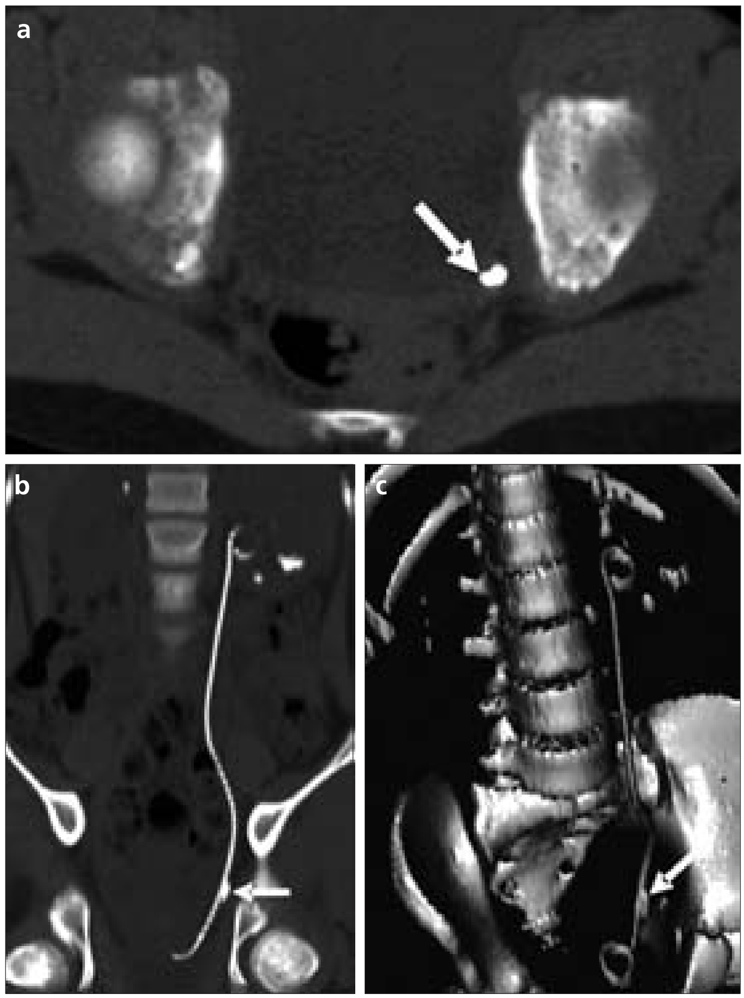

Figure 4. a–c. Axial **(a)**, coronal reconstructed **(b)**, and volume rendered **(c)** CT images of a 28-year-old female, who underwent double-J stenting and subsequent percutaneous nephrolithotomy procedures show a residual stone *(arrow)* within the left distal ureter. Note the benefit of bone windowing on axial and coronal reconstructed images in the depiction of residual stone *(arrow)* despite double-J stent.

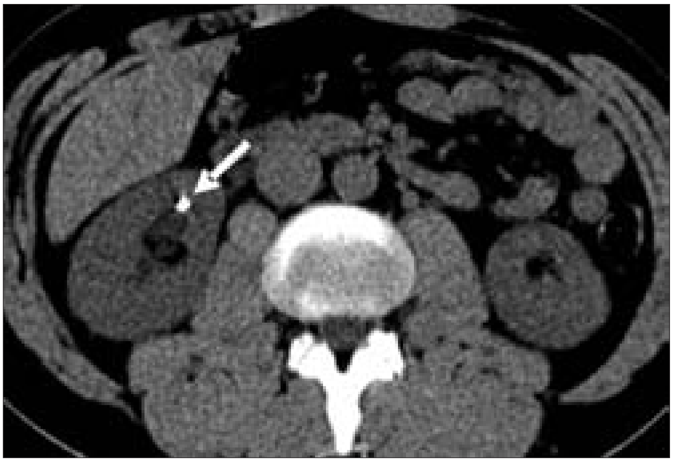

Figure 5. Axial unenhanced CT image shows a renal calculus *(arrow)* located at the middle portion of right renal collecting system.

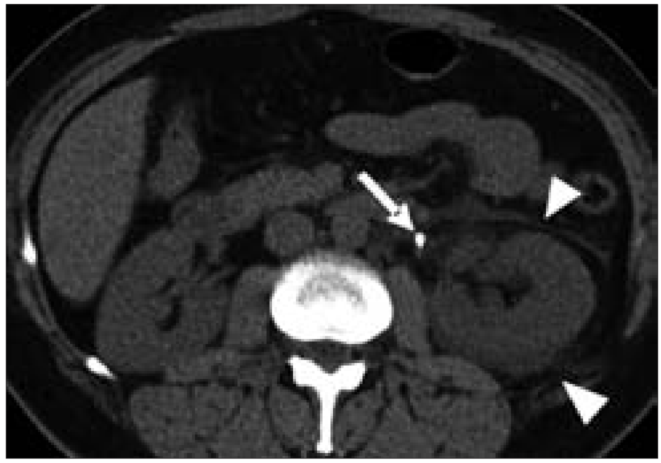

Figure 6. Axial unenhanced CT image of a 35-year-old female shows a left proximal ureter stone *(arrow)* and perinephric-periureteral stranding *(arrowheads)*, consistent with edema.

of tube current should be discussed. X-ray filters decrease “soft X-rays” which never reach the detectors and thus do not contribute to the image. Studies have shown that using effective X-ray filters causes a reduction in the radiation exposure and decrease in noise at a very-low-dose CT (21, 24). Automatic tube current modulation can be defined as a set of techniques that enable automatic adjustment of the tube current according to the size and attenuation characteristics of the body part being scanned and achieve constant CT image quality with lower radiation exposure (25). There are two methods used on CT scanners today: z-axis modulation and x-y axis (angular) modulation. The angular modulation technique modulates tube current on the basis of measured density of regional structures and absorption values of the interested organ. CARE Dose (Siemens Medical Systems, Erlangen, Germany) is the technique used on multi-detector row scanner for angular tube current modulation. Studies have shown that X-rays are much less attenuated in the anteroposterior direction than in the lateral direction (26–29). By using angular modulation technique, we can reduce anteroposterior X-rays without a marked effect on overall image noise by adjusting the tube current for each projection angle. Recent investigations in children, in whom angular modulation was used, showed 40–60% reduction in dose without loss of image quality (30). The z-axis modulation adjusts the tube current automatically to maintain a user-specified noise level in the image data. Z-axis modulation attempts to equalize noise in all slices independent of the patient’s size and anatomy. Auto mA (GE Healthcare, Milwaukee, Wisconsin, USA) is the technique used for z-axis modulation. A study showed that kidney stones smaller than 5 mm can be adequately evaluated by using “auto mA” modulation technique with a 56–75% reduction in radiation dose relative to the dose from a fixed-tube-current technique (31).

CT radiation dose optimization is a crucial issue especially for children and patients who have to undergo multiple CT examinations. As a result, it can be said that both the radiologists and manufacturers should focus on the strategies for limiting patient radiation dose and improve CT technology to provide necessary diagnostic image quality with reduced radiation dose.

Unenhanced MDCT findings of urinary stone disease

Primary findings

Without regarding the composition, renal stones can be readily detected on unenhanced MDCT images, since their attenuation is higher than any surrounding tissue. The attenuation of stones ranges between 200 to 1,700 HU on CT images (Fig. 5) (32). The dimension of the stone carries importance since it has a role in determination of the management method. Apart from moderate to big sized and staghorn stones, small ones which are often missed on direct radiographs can also be visualized within minor calyces or medullary pyramids.

The basic CT finding of acute ureteral obstruction secondary to urinary stone disease is the direct visualization of a stone within the ureter lumen. The diagnosis is confirmed if the ureter is found to be dilated above the level of a stone. Sometimes the diagnosis is challenging if patient has inadequate peritoneal fat tissue and has phleboliths along the course of ureters. Additionally, small size and low attenuation of the urinary stone, and respiratory artifacts may lead to confusion (33, 34). A stone within the ureter is identified by following the ureter inferior and superior to an area of calcification; beside this, secondary findings are common and include hydronephrosis, hydroureter, perinephric edema, enlargement of the kidney on the affected side and edema of the ureterovesical junction (Figs. 6, 7). Contralateral side may serve as a control helping to distinguish acute findings from normal findings (35).

Similar to renal stones, urinary bladder stones can also be detected on unenhanced MDCT images; however, ideally the urinary bladder should be full during the MDCT examination, thereby the overlying small bowel will be lifted and the ureterovesical junctions will be clearly identified. If the bladder remains empty during the examination, stones of the ureterovesical junction can be easily missed and sometimes large pelvic cysts may mimic a full bladder (Fig. 8) (36).

Secondary findings

Direct stone identification is diagnostic for lithiasis, but a stone may not

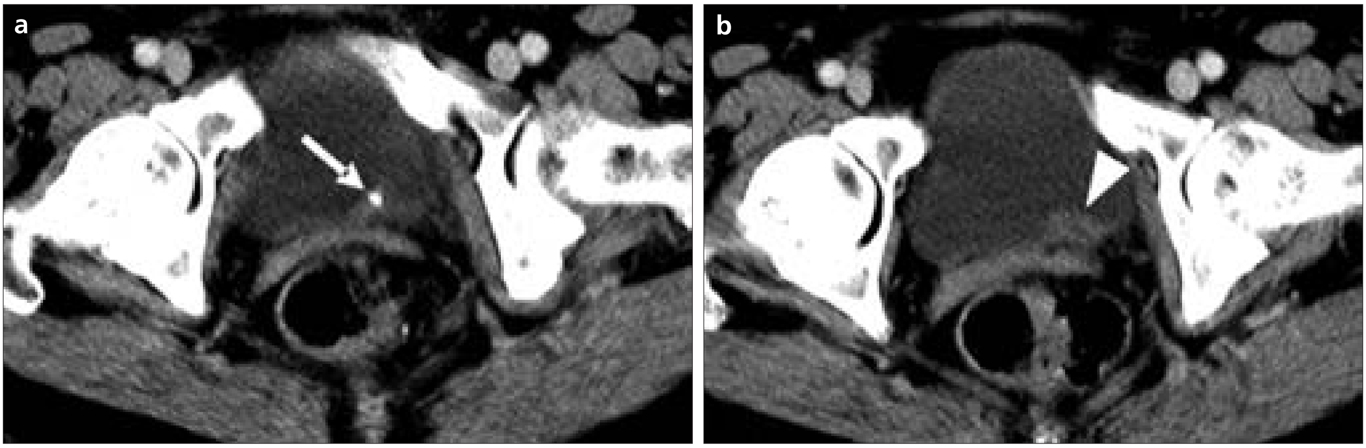

Figure 7. a, b. Axial contrast enhanced CT images of a 45-year-old male show a left ureterovesical junction stone (*arrow,* **a**) and secondary edema (*arrowhead,* **b**).

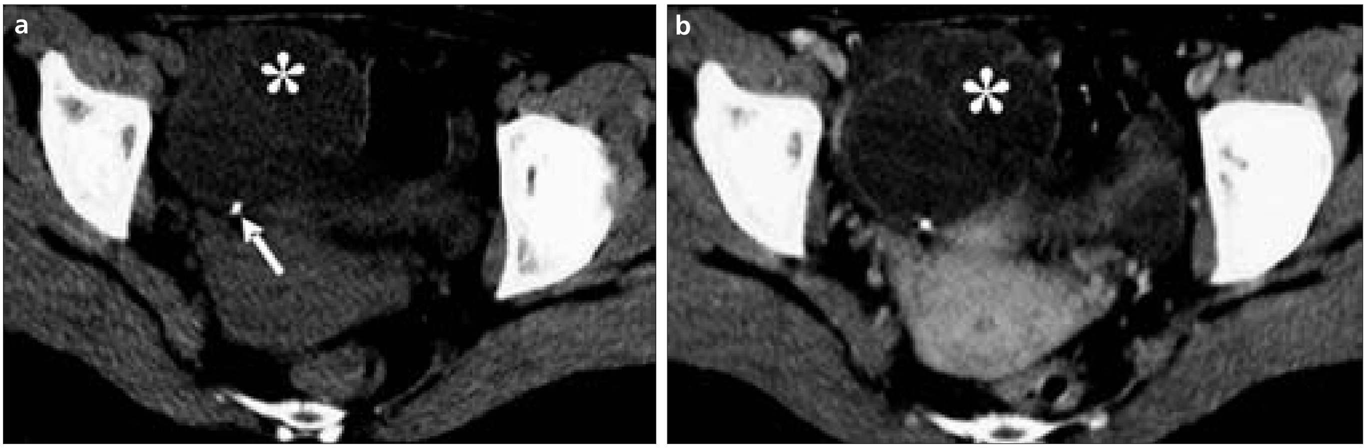

Figure 8. a, b. Axial unenhanced CT image **(a)** of a 26-year-old female with an empty urinary bladder shows an ovarian torsion *(asterisk)* with a calcification on the right side, mimicking a right ureterovesical junction stone *(arrow)*. Contrast enhanced CT image **(b)** confirms the diagnosis of ovarian torsion *(asterisk)*.

be easily identified due to its small size, low attenuation, respiratory movement artifacts, inadequacy of retroperitoneal fat tissue, phleboliths, and recent stone passage; under these circumstances, the presence of secondary signs carries great importance for prediction of the duration of stone disease and its management (37, 38). The secondary signs include asymmetric perinephric fat stranding, dilatation of the intrarenal collecting system, hydroureter, tissue rim sign, unilateral renal enlargement and pale kidney, and unilateral absence of white renal pyramids.

Asymmetric unilateral perinephric fat stranding

The changes in the perinephric space in the presence of urinary stone are thought to result from adaptation of the kidney to obstruction. Immediately after acute ureteral obstruction the intraluminal pressure of the collecting system increases and reaches to 3–5 times (39). Smooth muscle fibers of the urinary tract contracts as a response to this pressure increment; this results in increase of tension. Additionally, the amplitude of peristalsis increases; in case of persistent obstruction, smooth muscles of the urinary tract contract less forcefully, wall tension diminishes, peristalsis decreases. The escape of urine into the renal interstitium (pyelotubular backflow), across the renal pelvis into the renal sinus (pyelosinus backflow) or into the lymphatic system (pyelolymphatic backflow) or the renal venous system (pyelovenous backflow) play important roles in decompression of the intraluminal pressure (40). As proposed by Kunin, lymphatic flow in the perinephric space results from elevated intrarenal venous pressure, and venous stasis, pyelosinus and pyelovenous backflow may contribute to perinephric stranding (Fig. 6) (40, 41).

Elevated pressure in the collecting system is considered to be the most important force that causes a stone to move down the ureter; this occurs during acute phase of the obstruction. This is probably why an increased degree of perinephric fat stranding and the presence of perinephric fluid collection are associated with an increased rate of spontaneous stone passage. Hydronephrosis reflects a subacute to chronic phase obstruction; moreover, a longer duration of passage and hydronephrosis indicate decrement of frequency of peristalsis and lowered probability of spontaneous stone passage (Fig. 9). A smaller stone size and a higher degree of perinephric fat stranding or an increased amount of perinephric stranding and fluid are associated with a higher likelihood of

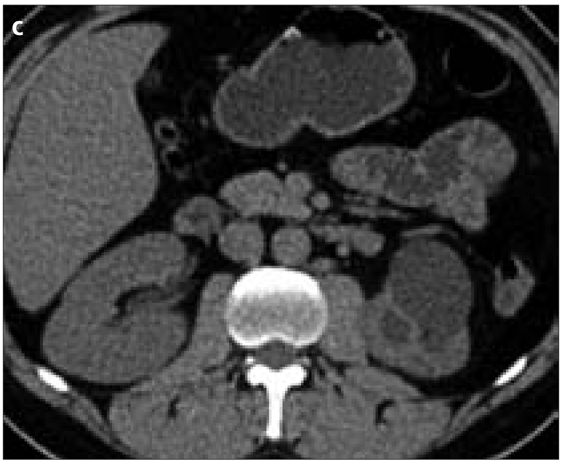

Figure 9. a–c. Axial unenhanced CT image **(a)** shows a stone located at the lower third of the left ureter *(arrow)*. Coronal reconstructed CT image **(b)** shows significant left hydroureteronephrosis *(arrowhead)* without perinephric and periureteral edema. Axial CT image of the left kidney **(c)** shows chronic changes in the kidney. All findings are consistent with the chronic phase of obstruction.

spontaneous stone passage (Fig. 10) (40, 41).

Dilatation of the intrarenal collecting system

Evaluation of the renal collecting system is important for determination of the obstruction and it should focus on the renal sinus in the upper and lower poles since differentiation from extrarenal pelvis may be challenging. There is less variation in the intrarenal portion of the renal collecting system; that is why collecting system is best identified in upper and lower poles. Dilated calyces appear as round fluid-filled structures that obliterate the renal sinus fat (Fig. 11).

Hydroureter

Ureteral dilatation is generally readily detected unless phleboliths are present and intraabdominal fat tissue is inadequate. Once the presence of hydroureter is established, ureter should be followed throughout its course. Evaluation should be made for the presence of calculi, mass and/or other extrinsic causes leading to obstruction. Identification of ureter is often diffi-

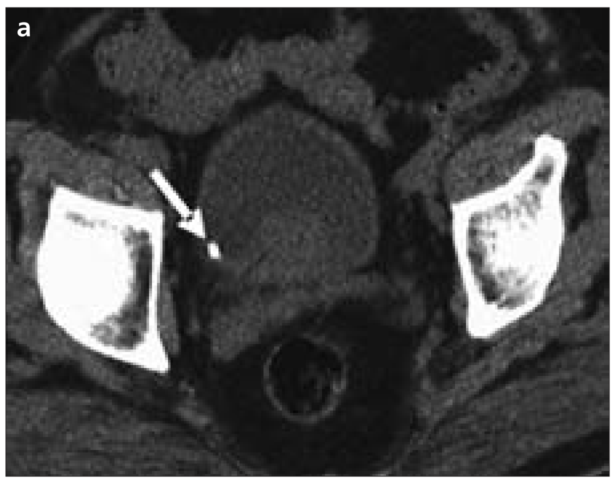

Figure 10. a, b. Axial unenhanced CT image **(a)** of a 47-year-old male shows a right ureterovesical junction stone *(arrow)*. Coronal reconstructed CT image **(b)** shows mild-to-moderate hydroureteronephrosis and minimal perinephric edema. All findings are consistent with a higher likelihood of spontaneous stone passage.

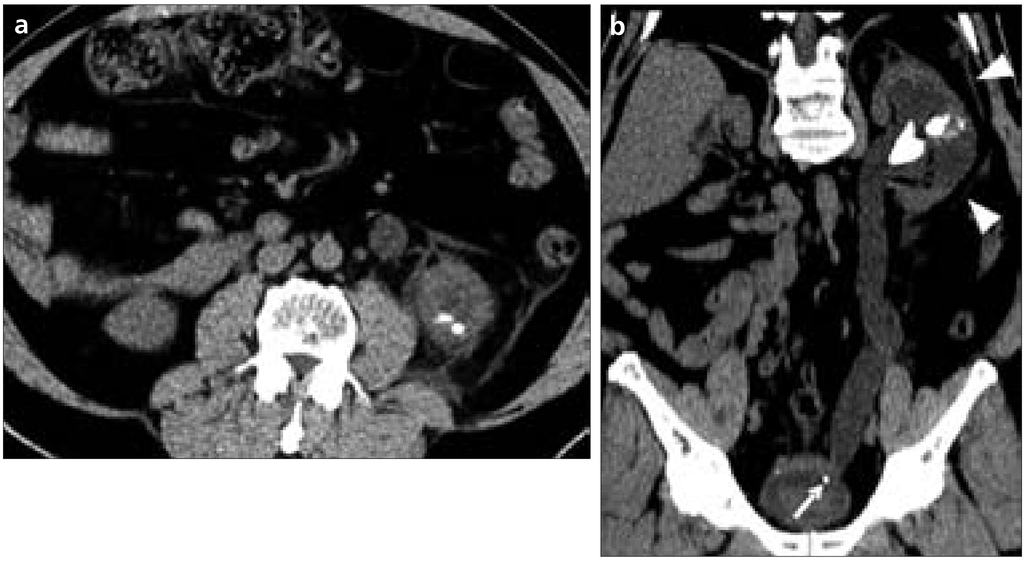

Figure 11. a, b. Axial unenhanced CT image **(a)** of a 40-year-old male shows left kidney stones. Coronal reconstructed CT image **(b)** shows a left staghorn kidney and ureterovesical junction stones *(arrow)*, dilated calyces, obliteration of the left renal sinus fat and perinephric edema *(arrowheads)*.

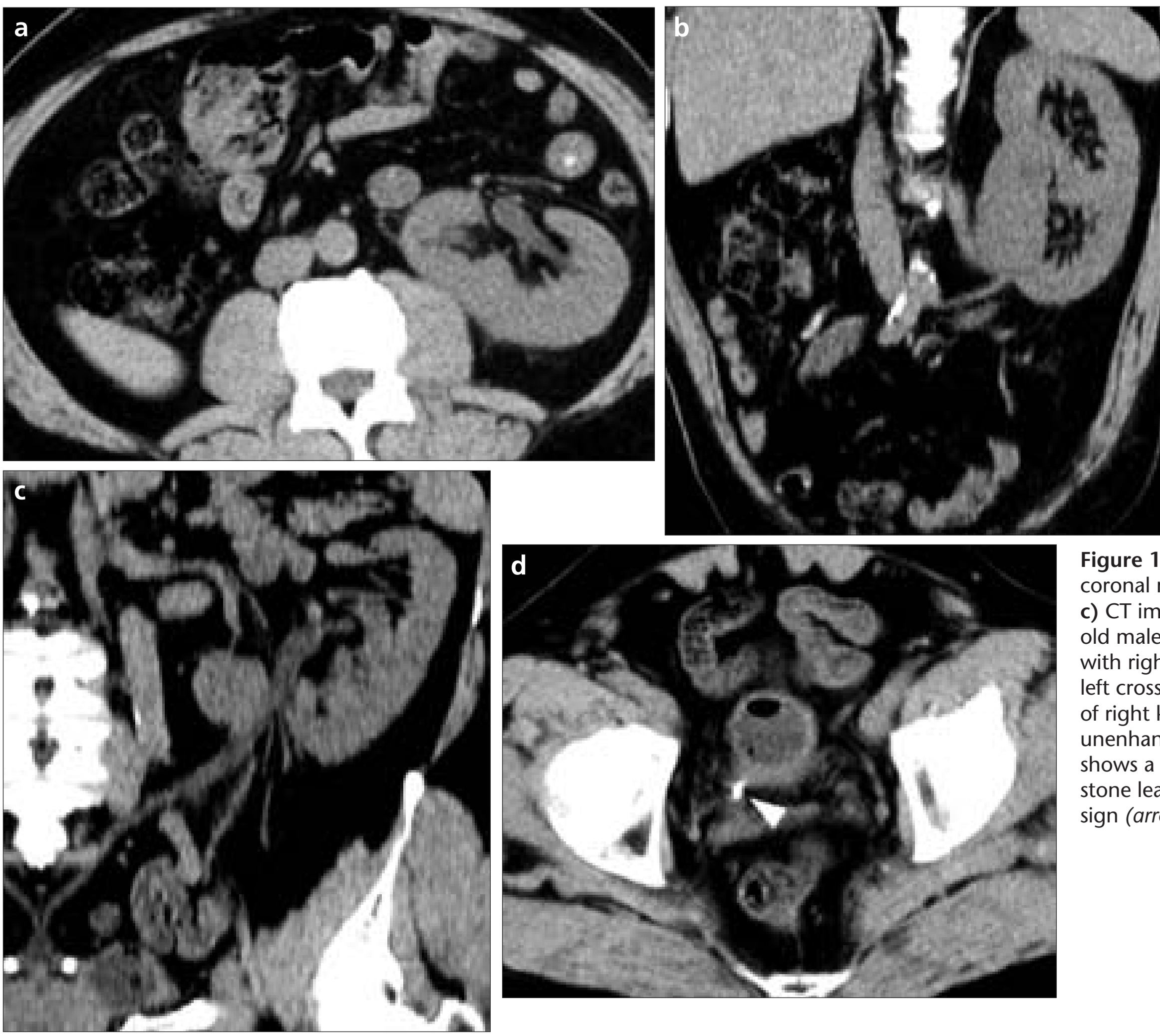

Figure 12. a–d. Axial **(a)** and coronal reconstructed **(b, c)** CT images of a 40-year-old male, who presented with right flank pain, shows left crossed-fused ectopia of right kidney. Axial pelvic unenhanced CT image **(d)** shows a right lower ureter stone leading to tissue rim sign *(arrowhead)*.

cult; viewing on a workstation in cine mode is often useful especially in challenging cases (Figs. 10, 11).

Tissue rim sign

The rim sign is a circumferential halo of soft tissue attenuation around an abdominal or pelvic calcification; this sign indicates that the calcification is ureteral (42, 43). This finding usually helps distinction of stone obstruction from phleboliths (Fig. 12).

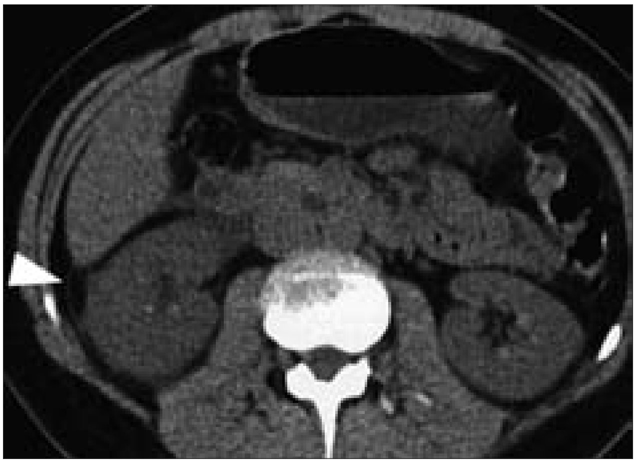

Figure 13. Axial unenhanced CT image of a 33-year-old female, who presented with right flank pain, shows unilateral absence of the white renal pyramids on the right side. Additionally right perinephric stranding is seen *(arrowhead)*, and findings are consistent with obstruction secondary to calculus.

Figure 14. a, b. Axial unenhanced CT image **(a)** of a 43-year-old female shows enlargement of the right kidney and dilatation of its collecting system. Moreover, right perinephric stranding is seen (*arrowhead,* **a**). Coronal reconstructed CT image **(b)** shows a right distal ureter stone *(arrow)* and proximal hydroureteronephrosis.

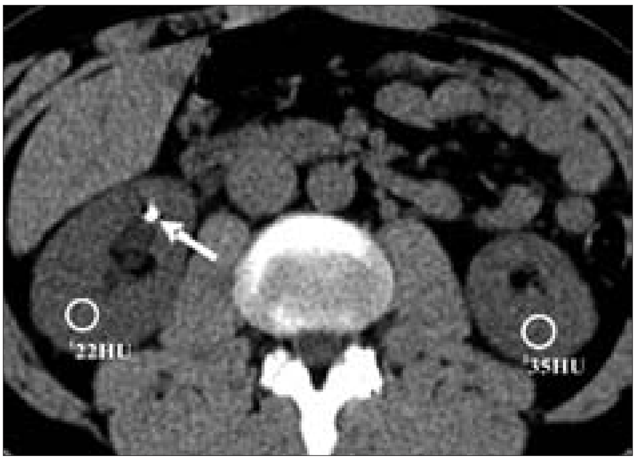

Figure 15. Axial unenhanced CT image of a 23-year-old male (the same patient as in Fig. 5) shows a right pale kidney representing renal edema secondary to obstruction of a urinary stone *(arrow)*.

Unilateral absence of white renal pyramids

Recently, unilateral absence of white renal pyramids is described as an indicator of urinary tract obstruction. Ureteral obstruction may lead to tubular hydronephrosis which may result in a relative decrease in attenuation of the renal pyramids on the affected site compared with the unaffected side which remains normal (Fig. 13) (44, 45).

Unilateral renal enlargement and pale kidney

Kidney size is usually measured larger on the affected side when compared with the contralateral side; this is a result of the dilatation of the renal collecting system and edema. Kidney edema indicates the organ's response to the obstruction and it can be defined as a density difference between the two kidneys on unenhanced CT scans which is more than 5 HU, this sign can be useful in case of difficulty during differentiation of a ureteral calculus from a phlebolith (7) (Figs. 14, 15).

Pitfalls

There are many pitfalls that may occur in the identification of urinary stone disease on unenhanced MDCT images; most are related to calcifications that simulate calculi. Calcifications of the iliac vessels may be difficult to differentiate from an adjacent ureter stone; by re-evaluating the images in cine mode at a workstation, ureterolithiasis can be differentiated from such calcifications. Rarely, in selected cases intravenous contrast material administration may also be helpful for differentiation.

Presence of phleboliths is a major problem for lower ureteral and ureterovesical junction stones since they are common in this area; again by using the workstation for cine mode re-evaluation differentiation can be made. Moreover, the rim and comet tail signs are described for evaluation of pelvic calcifications in case of confusion on their relationship with the ureter (43, 45, 46). The rim sign is a thin circumferential layer of soft tissue attenuation around an abdominal or pelvic calcification, this attenuation indicates that the calcification represents ureteral edema with a stone. On

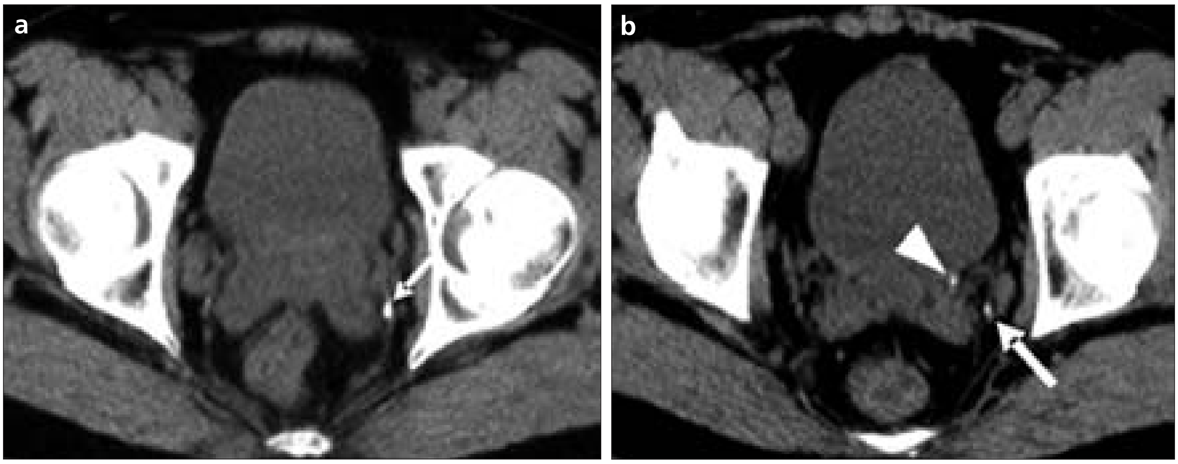

Figure 16. a, b. Axial unenhanced CT images of a 34-year-old male, who presented with left flank pain show comet tail sign representing a phlebolith within the left pelvis (*arrows.* **a, b**). A left ureterovesical junction stone is also seen (*arrowhead,* **b**).

Figure 17. Axial unenhanced CT image of a 65-year-old male, who presented with bilateral flank pain and dysuria show bilateral iliac vessel *(arrow)* and seminal vesicle *(arrowhead)* calcifications mimicking ureteral stones.

the other hand, the comet tail sign is a linear soft tissue attenuation extending from an abdominal or pelvic calcification indicating that the calcification is a phlebolith (Figs. 16, 17) (35, 46). If all of these strategies are useless, intravenous contrast material injection can be done for differentiation.

Besides calcifications, some other conditions may interfere with the establishment of the exact diagnosis by mimicking hydronephrosis. These include parapelvic renal cysts, extrarenal pelvis, vesicoureteral reflux disease, and transitional cell tumors. Large pelvic cysts may mimic a full bladder in case of an empty bladder during unenhanced MDCT examination (Fig. 8).

A potential and often underestimated pitfall is the incomplete area scanned during the examination. Images should be acquired from the top of the kidneys to the lower border of the pubic symphysis. Occasionally stones may be present in the inferior part of the bladder or within a urethral diverticulum in women. These stones can be missed due to incomplete coverage (36).

Can stone composition be estimated?

Stone composition affects the efficacy of extracorporeal shock wave lithotripsy (ESWL) (47). Stones composed of calcium oxalate and cystine typically do not respond well to ESWL. Identification of such stones by MDCT via attenuation measurement may prevent unnecessary ESWL attempts and divert treatment to endoscopic approach. Nakada et al. proposed advantage of attenuation/size ratio of stone in depicting composition of urinary stones (48). They measured HU attenuation level for each pixel representing the stone, and took the highest measured value, then divided the value by the size of the stone. As a result, they found out that if a stone had an attenuation/size ratio of lower than 80, it could be a uric acid stone; if the ratio was found to be greater than 80, this indicated a non-uric acid stone (48). Deveci et al. concluded in an *in vitro* study that chemical compositions of both pure and mixed stones can be determined by using multi-slice CT (49).

Alternative diagnoses

Almost 50% of patients with acute flank pain have no urinary stone on CT examinations; among them an alternative cause of flank pain is identified in nearly one third of cases (36). Some of the alternative diagnoses are congenital renal anomalies, infections (appendicitis, diverticulitis, pancreatitis, mesenteric lymphadenitis, cholecystitis, colitis, pyelonephritis), aortic aneurysm and dissection, ovarian cysts and neoplasms (renal, uterine and adnexal masses) (Figs. 18, 19) (11, 50, 51).

When should the intravenous contrast be given?

Intravenous contrast is not routinely given for CT imaging of renal colic, but reaching a correct diagnosis and characterization of tumoral and cystic lesions can be challenging in patients with equivocal unenhanced CT findings. Indications for contrast-enhanced CT evaluation (based on unenhanced CT findings) are: i) presence of unilateral perinephric stranding without hydroureteronephrosis with or without renal enlargement (acute renal infarction, renal vein thrombosis, acute pyelonephritis); ii) significant hypo-/hyperdense perirenal collection (urinoma, hematoma) with or without the

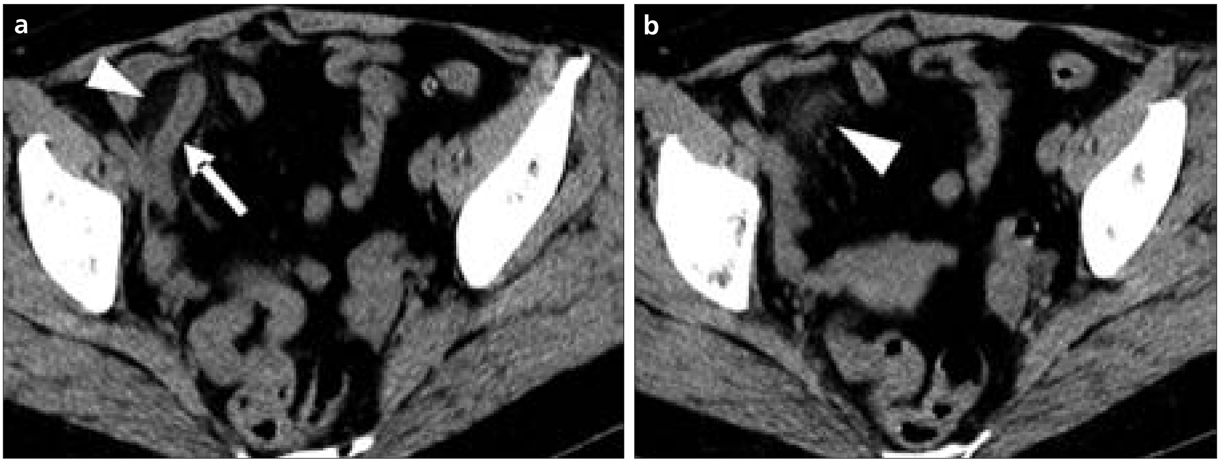

Figure 18. a, b. Axial unenhanced CT images of a 21-year-old male, who presented with right flank pain radiating towards groin region, shows a dilated tubular intestinal segment (*arrow,* **a**) and adjacent mesenteric inflammation (*arrowheads,* **a, b**) consistent with acute appendicitis.

Figure 19. Axial unenhanced CT image of a 56-year-old male, who presented with left flank pain and gross hematuria shows a large mass in the anterior part of the urinary bladder *(asterisk)* leading to left hydronephrosis *(arrowhead)*. Additionally a loculated fluid collection *(arrow)* is seen at the right side of the urinary bladder.

presence of hydroureteronephrosis; iii) presence of a mass or complicated cyst with/without calculus; iv) negative unenhanced CT findings in a patient with unexplained hematuria (52). Common clinical conditions requiring contrast-enhanced CT after unenhanced CT scan in a patient presenting with flank pain and hematuria are infections, neoplasms, renal cyst complications, vascular lesions, urinoma and acute perirenal hematoma, of which imaging findings are already defined elsewhere (51–55).

Conclusion

Unenhanced CT is a widely used imaging modality for the evaluation of urinary stone disease. Primary imaging findings, secondary signs and potential pitfalls of unenhanced CT findings carry considerable importance in terms of accurate diagnosis and decision-making for treatment selection. Additionally, awareness of radiation exposure reduction strategies, patient protection and correct intravenous contrast material administration judgment will both yield a safer and more beneficial road to diagnosis.

References

1. Hiatt RA, Dales LG, Friedman GD, Hunkeler EM. Frequency of urolithiasis in a prepaid medical care program. Am J Epidemiol 1982; 115:255–265.
2. Tamm EP, Silverman PM, Shuman WP. Evaluation of the patient with flank pain and possible ureteral calculus. Radiology 2003; 228:319–329.
3. Heidenreich A, Desgrandschamps F, Terrier F. Modern approach of diagnosis and management of acute flank pain: review of all imaging modalities. Eur Urol 2002; 41:351–362.
4. Yilmaz S, Sindel T, Arslan G, et al. Renal colic: comparison of spiral CT, US and IVU in the detection of ureteral calculi. Eur Radiol 1998; 8:212–217.
5. Pietrow PK, Karellas ME. Medical management of common urinary calculi. Am Fam Physician 2006; 74:86–94.
6. Dunnick RN, Sandler CM, Newhouse JH, Amis ES Jr. Nephrocalcinosis and nephrolithiasis. In: Textbook of uroradiology. 3rd ed. Philadelphia: Saunders, 1994; 435–467.
7. Georgiades CS, Moore CJ, Smith DP. Differences of renal parenchymal attenuation for acutely obstructed and unobstructed kidneys on unenhanced helical CT: a useful secondary sign? AJR Am J Roentgenol 2001; 176:965–968.
8. Rao PN. Imaging for kidney stones. World J Urol 2004; 22:323–327.
9. Smith RC, Rosenfield AT, Choe KA, et al. Acute flank pain: comparison of non-contrast-enhanced CT and intravenous urography. Radiology 1995; 194:789–794.
10. Kirpalani A, Khalili K, Lee S, Haider MA. Renal colic: comparison of use and outcomes of unenhanced helical CT for emergency investigation in 1998 and 2002. Radiology 2005; 236:554–558.
11. Chen MY, Zagoria RJ, Saunders HS, Dyer RB. Trends in the use of unenhanced helical CT for acute urinary colic. AJR Am J Roentgenol 1999; 173:1447–1450.
12. Mindelzun RE, Jeffrey RB. Unenhanced helical CT for evaluating acute abdominal pain: a little more cost, a lot more information. Radiology 1997; 205:43–45.
13. Hartman GW, Hattery RR, Witten DM, Williamson B Jr. Mortality during excretory urography: Mayo Clinic experience. AJR Am J Roentgenol 1982; 139:919–922.
14. Sohaib SA, Peppercorn PD, Horrocks JA, Keene MH, Kenyon GS, Reznek RH. The effect of decreasing mAs on image quality and patient dose in sinus CT. Br J Radiol 2001; 74:157–161.
15. Takahashi M, Maguire WM, Ashtari M, et al. Low-dose spiral computed tomography of the thorax: comparison with the standard-dose technique. Invest Radiol 1998; 33:68–73.
16. Naidich DP, Marshall CH, Gribbin C, Arams RS, McCauley DI. Low-dose CT of the lungs: preliminary observations. Radiology 1990; 175:729–731.
17. Kalra MK, Prasad S, Saini S, et al. Clinical comparison of standard-dose and 50% reduced-dose abdominal CT: effect on image quality. AJR Am J Roentgenol 2002; 179:1101–1106.
18. Kamel IR, Hernandez RJ, Martin JE, Schlesinger AE, Niklason LT, Guire KE. Radiation dose reduction in CT of the pediatric pelvis. Radiology 1994; 190:683–687.

19. Heneghan JP, McGuire KA, Leder RA, Delong DM, Yoshizumi T, Nelson RC. Helical CT for nephrolithisis and ureterolithiasis: comparison of conventional and reduced radiation-dose techniques. Radiology 2003; 229:575–580.
20. Diel J, Perlmutter S, Venkataramanan N, Mueller R, Lane MJ, Katz DS. Unenhanced helical CT using increased pitch for suspected renal colic: an effective technique for radiation dose reduction? J Comput Assist Tomogr 2000; 24:795–801.
21. Liu W, Esler SJ, Kenny BJ, Goh RH, Rainbow AJ, Stevenson GW. Low-dose nonenhanced helical CT of renal colic: assessment of ureteric stone detection and measurement of effective dose equivalent. Radiology 2000; 215:51–54.
22. Kalra MK, Prasad S, Saini S, et al. Clinical comparison of standard-dose and 50% reduced-dose abdominal CT: effect on image quality. AJR Am J Roentgenol 2002; 179:1101–1106.
23. Donnelly LF, Emery KH, Brody AS, et al. Minimizing radiation dose for pediatric body applications of single-detector helical CT: strategies at a large children's hospital. AJR Am J Roentgenol 2001; 176:303–306.
24. Toth TL. Dose reduction opportunities for CT scanners. Pediatr Radiol 2002; 32:261–267.
25. Kalra MK, Maher MM, Toth TL, et al. Techniques and applications of automatic tube current modulation for CT. Radiology 2004; 233:649–657.
26. Greess H, Wolf H, Baum U, et al. Dose reduction in computed tomography by attenuation-based on-line modulation of tube current: evaluation of six anatomical regions. Eur Radiol 2000; 10:391–394.
27. Kalender WA, Wolf H, Suess C, Gies M, Greess H, Bautz WA. Dose reduction in CT by on-line tube current control: principles and validation on phantoms and cadavers. Eur Radiol 1999; 9:323–328.
28. Gies M, Kalender WA, Wolf H, Suess C. Dose reduction in CT by anatomically adapted tube current modulation. I. Simulation studies. Med Phys 1999; 26:2235–2247.
29. Kalender WA, Wolf H, Suess C. Dose reduction in CT by anatomically adapted tube current modulation. II. Phantom measurements. Med Phys 1999; 26:2248–2253.
30. Greess H, Nomayr A, Wolf H, et al. Dose reduction in CT of children by an attenuation-based on-line modulation of tube current (CARE dose). Eur Radiol 2002; 12:1571–1576.
31. Kalra MK, Maher MM, D'Souza RV, et al. Detection of urinary tract stones using z-axis automatic tube current modulation technique with low radiation dose: phantom and clinical studies. Radiology 2005; 235:523–529.
32. Newhouse JH, Prien EL, Amis ES Jr, Dretler SP, Pfister RC. Computed tomographic analysis of urinary calculi. AJR Am J Roentgenol 1984; 142:545–548.
33. Smith RC, Verga M, Dalrymple N, McCarthy S, Rosenfield AT. Acute ureteral obstruction: value of secondary signs of helical unenhanced CT. AJR Am J Roentgenol 1996; 167:1109–1113.
34. Goldman SM, Faintuch S, Ajzen SA, et al. Diagnostic value of attenuation measurements of the kidney on unenhanced helical CT of obstructive ureterolithiasis. AJR Am J Roentgenol 2004; 182:1251–1254.
35. Katz DS, Hines J, Rausch DR, et al. Unenhanced helical CT for suspected renal colic. AJR Am J Roentgenol 1999; 173:425–430.
36. Colistro R, Torreggiani WC, Lyburn ID, et al. Unenhanced helical CT in the investigation of acute flank pain. Clin Radiol 2002; 57:435–441.
37. Varanelli MJ, Coll DM, Levine JA, Rosenfield AT, Smith RC. Relationship between duration of pain and secondary signs of obstruction of the urinary tract on unenhanced helical CT. AJR Am J Roentgenol 2001; 177:325–330.
38. Akay H, Akpinar E, Ergun O, Ozmen CA, Haliloglu M. Unenhanced multidetector CT evaluation of urinary stones and secondary signs in pediatric patients. Diagn Interv Radiol 2006; 12:147–150.
39. Rose JG, Gillenwater JY. Pathophysiology of ureteral obstruction. Am J Physiol 1973; 225:830–837.
40. Takahashi N, Kawashima A, Ernst RD, et al. Ureterolithiasis: can clinical outcome be predicted with unenhanced helical CT? Radiology 1998; 208:97–102.
41. Kunin M. Bridging septa of the perinephric space: anatomic, pathologic, and diagnostic considerations. Radiology 1986; 158:361–365.
42. Guest AR, Cohan RH, Korobkin M, et al. Assessment of the clinical utility of the rim and comet-tail signs in differentiating ureteral stones from phleboliths. AJR Am J Roentgenol 2001; 177:1285–1291.
43. Heneghan JP, Dalrymple NC, Verga M, Rosenfield AT, Smith RC. Soft-tissue „rim" sign in the diagnosis of ureteral calculi with use of unenhanced helical CT. Radiology 1997; 202:709–711.
44. Ege G, Akman H, Kuzucu K, Yildiz S. Acute ureterolithiasis: incidence of secondary signs on unenhanced helical CT and influence on patient management. Clin Radiol 2003; 58:990–994.
45. Kawashima A, Sandler CM, Boridy IC, Takahashi N, Benson GS, Goldman SM. Unenhanced helical CT of ureterolithiasis: value of the tissue rim sign. AJR Am J Roentgenol 1997; 168:997–1000.
46. Bell TV, Fenlon HM, Davison BD, Ahari HK, Hussain S. Unenhanced helical CT criteria to differentiate distal ureteral calculi from pelvic phleboliths. Radiology 1998; 207:363–367.
47. Dretler SP. Stone fragility-a new therapeutic distinction. J Urol 1988; 139:1124–1127.
48. Nakada SY, Hoff DG, Attai S, Heisey D, Blankenbaker D, Pozniak M. Determination of stone composition by noncontrast spiral computed tomography in the clinical setting. Urology 2000; 55: 816–819.
49. Deveci S, Coşkun M, Tekin MI, Peşkircioglu L, Tarhan NC, Ozkardeş H. Spiral computed tomography: role in determination of chemical compositions of pure and mixed urinary stones—an in vitro study. Urology 2004; 2:237–240.
50. Koroglu M, Wendel JD, Ernst RD, Oto A. Alternative diagnoses to stone disease on unenhanced CT to investigate acute flank pain. Emerg Radiol 2004; 10:327–333.
51. Rucker CM, Menias CO, Bhalla S. Mimics of renal colic: alternative diagnoses at unenhanced helical CT. Radiographics 2004; 24(Suppl 1):S11–28.
52. Akpinar E, Turkbey B, Eldem G, Karcaaltincaba M, Akhan O. When do we need contrast-enhanced CT in patients with vague urinary system findings on unenhanced CT? Emerg Radiol 2009; 16:97–103.
53. Titton RL, Gervais DA, Hahn PF, Harisinghani MG, Arellano RS, Mueller PR. Urine leaks and urinomas: diagnosis and imaging-guided intervention. Radiographics 2003; 23:1133–1147.
54. Krinsky G. Unenhanced helical CT in patients with acute flank pain and renal infarction: the need for contrast material in selected cases. AJR Am J Roentgenol 1996; 167:282–283.
55. Israel GM, Hindman N, Bosniak MA. Evaluation of cystic renal masses: comparison of CT and MR imaging by using the Bosniak classification system. Radiology 2004; 231:365–371.